POLITECNICO DI TORINO
Repository ISTITUZIONALE

Adaptive T-Detector for Intercarrier Interference Mitigation in Spectrally Efficient Frequency Modulation Systems

Original
Adaptive T-Detector for Intercarrier Interference Mitigation in Spectrally Efficient Frequency Modulation Systems / Magnaldi, M., Montorsi, G.. - (2026). (Next Generation Communications (NextGCom) conference 2026 Kefalonia (Gre) 28-30 Settembre 2026).

Availability:
This version is available at: 11583/3015097 since: 2026-09-02T14:35:01Z

Publisher:
IEEE

Published
DOI:

Terms of use:

This article is made available under terms and conditions as specified in the corresponding bibliographic description in the repository

Publisher copyright
IEEE postprint/Author's Accepted Manuscript

©2026 IEEE. Personal use of this material is permitted. Permission from IEEE must be obtained for all other uses, in any current or future media, including reprinting/republishing this material for advertising or promotional purposes, creating new collecting works, for resale or lists, or reuse of any copyrighted component of this work in other works.

(Article begins on next page)

18 October 2026

Adaptive T-Detector for Intercarrier Interference Mitigation in Spectrally Efficient Frequency Modulation Systems

Martina Magnaldi and Guido Montorsi
Dep. of Elec. and Telecomm. (DET), Politecnico di Torino, Italy
martina.magnaldi@polito.it, guido.montorsi@polito.it

***Abstract*—In this work, we show that the T-Detector, originally developed for time-domain inter-symbol interference (ISI), generalizes to frequency-domain intercarrier interference (ICI) without any modification to its fundamental detection procedure, and apply it to Spectrally Efficient Frequency Division Multiplexing (SEFDM) systems, where bandwidth compression introduces significant ICI. The shortening filter is reinterpreted to operate across subcarriers rather than time samples, and a trainable one-tap equalizer is introduced to separate the unknown, random fading distortion from the deterministic ICI structure. The proposed receiver architecture is channel- and modulation-agnostic and integrates channel shortening, frequency-domain equalization, maximum-likelihood sequence detection, and log-likelihood computation for soft decoding, with a computational complexity comparable to that of classical detection schemes. Numerical results demonstrate that the proposed approach proves effective in SEFDM systems, achieving near-optimal performance in both mutual information (MI) and bit-error rate (BER). Finally, we analyze the operational limits of the T-Detector in terms of the maximum bandwidth compression factor for which the achievable MI can still be attained at high SNR.**

***Index Terms*—BCJR algorithm, model-based neural networks, Maximum Likelihood equalization, channel shortening, SEFDM.**

I. Introduction

Spectrally Efficient Frequency Division Multiplexing (SEFDM) [1] is a non-orthogonal multicarrier modulation scheme inspired by Faster-Than-Nyquist (FTN) signaling, where reduced subcarrier spacing improves spectral efficiency at the cost of intercarrier interference (ICI). Symbol generation and waveform synthesis for SEFDM have been analyzed in [2], while a comprehensive overview of waveform design, equalization, and detection is provided in [3]. Several detection strategies have been proposed to mitigate ICI, including FFT-based trellis receivers [4], [5], lattice-based detectors [6], zero-forcing and Viterbi-based schemes [7], iterative interference cancellation [8]–[10]. Low-complexity alternatives include the Fixed-Complexity Sphere Decoder (FSD) [11], which offers near-optimal performance with reduced complexity. More recent approaches explore message-passing frameworks: [12] develops a Gaussian message-passing (GMP) receiver for coded multicarrier faster-than-Nyquist (MFTN) systems that considers only neighboring time-frequency interference to lower computational cost, while [13] proposes a Forney-style factor-graph detection algorithm with a novel scheduling criterion that avoids matrix inversions and spectral decompositions.

In this work, we apply our model-based neural detector, the T-Detector, to SEFDM systems. In previous studies [14]–[16], we introduced this adaptive, fully trainable detector for single-carrier inter-symbol interference (ISI) channels, built around the T-BCJR [17]. The architecture is based on the channel shortening approach [18], [19], employing a convolutional layer that emulates the shortening filter preceding the T-BCJR. This design enables end-to-end training from the detector output log-likelihoods (LLs), binary or non-binary, allowing adaptation to unknown channels and constellations while achieving near-optimal performance in static and slowly varying channels with appropriate pilot densities.

Our contribution is a demonstration that a single CSI-free trainable architecture can be reinterpreted to handle two structurally different impairments, ISI and ICI, through the same channel-shortening principle. In SEFDM, where ICI dominates and ISI is mitigated by the cyclic prefix (CP), the shortening filter is reinterpreted to operate across frequency-domain samples rather than time-domain ones, with the only architectural addition being a trainable equalizer to decouple the unknown per-subcarrier fading distortion from the deterministic ICI structure. Channel estimation is inherently learned during the initial training phase, allowing robust operation in AWGN and fading channels without explicit CSI, distinguishing the proposed approach from most existing SEFDM detectors. The detector can be seamlessly integrated with soft-input capacity-achieving binary decoders, as in [14].

The remainder of the paper is organized as follows. In Section II, we introduce the system model, while in Section III we present the T-BCJR and the T-Detector. Section IV explains how the T-Detector architecture is extended to address impairments caused by both ICI and fading channels. Section V discusses the relationship between the proposed approach and conventional equalization, together with the operational limits of the T-Detector in terms of compression factor and block processing. Simulation results for static and time-varying AWGN and fading channels are presented in Section VI. Finally, Section VII concludes the paper and outlines future work.

II. System Model

We consider a SEFDM system composed of N subcarriers, where the subcarrier spacing is reduced by a compression

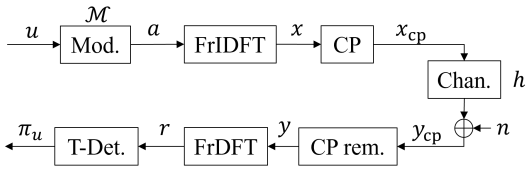

Fig. 1: Block diagram of the SEFDM system model.

factor $\alpha < 1$ with respect to conventional OFDM. The compression factor follows the relation $\alpha = \Delta f\, T$, where Δf is the spacing between adjacent subcarriers and T is the symbol duration. Thus, SEFDM violates the OFDM orthogonality condition, $\Delta f = 1/T$. By compressing the subcarrier spacing, SEFDM increases the spectral efficiency by a factor $1/\alpha$.

The discrete-time SEFDM symbol can be expressed as:

$$x_k = \frac{1}{\sqrt{N}} \sum_{n=0}^{N-1} a_n\, e^{j2\pi n\alpha \frac{k}{N}}, \qquad k = 0, 1, ..., N-1. \tag{1}$$

where a_n denotes the nth input symbol and $1/\sqrt{N}$ ensures normalization. The expression in Eq. (1) can be written in matrix form as:

$$x_0^{N-1} = \mathbf{F}_{N,\alpha}^H\, a_0^{N-1}, \quad [\mathbf{F}_{N,\alpha}]_{n,k} = \frac{1}{\sqrt{N}} e^{-j2\pi nk\alpha/N}, \tag{2}$$

where $x_0^{N-1} = [x_0, x_1, ..., x_{N-1}]^T$, $a_0^{N-1} = [a_0, a_1, ..., a_{N-1}]^T$, and $\mathbf{F}_{N,\alpha}$ is the $N \times N$ *fractional discrete Fourier transform* (FrDFT) matrix.

We first consider an ideal, noise-free channel. Applying the FrDFT to the transmitted signal yields:

$$r_0^{N-1} = \mathbf{F}_{N,\alpha}\, x_0^{N-1}. \tag{3}$$

The kth component of $\mathbf{r}_0^{N-1}$ can be expressed as:

$$r_k = \sum_{n=0}^{N-1} a_n\, g_{n,k}, \tag{4}$$

$$g_{n,k} = \frac{1}{N} \sum_{m=0}^{N-1} e^{j2\pi m(n-k)\alpha/N}, \quad k = 0, \ldots, N-1. \tag{5}$$

Each spectral sample r_k is a linear combination of all transmitted symbols a_n. The coefficients $g_{n,k}$ quantify the ICI, introduced by SEFDM modulation, as illustrated in Fig. 2. It becomes clear that subcarriers do not contribute uniformly to the interference: the nearest neighbors dominate the ICI, whereas those farther away have only a minor effect and can often be disregarded. However, as the bandwidth is increasingly compressed, the influence of more distant subcarriers grows, requiring a larger set of them to be considered.

We now consider a static tapped delay line (TDL) fading channel with a channel impulse response (CIR) vector h of length L_C, and additive white Gaussian noise w. The cyclic prefix (CP) is assumed to be longer than the CIR, so that ISI is completely removed. After CP removal, the discrete received baseband signal is as follows:

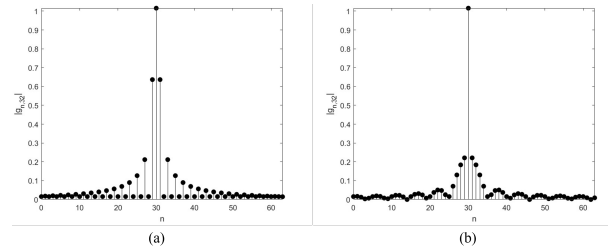

Fig. 2: Absolutes values of $g_{n,32}$ for $N = 64$, (a) $\alpha = 0.5$, (b) $\alpha = 0.8$.

$$y_0^{N-1} = \mathbf{H}\, x_0^{N-1} + w_0^{N-1}, \tag{6}$$

where $\mathbf{H}$ is a circulant matrix containing circularly shifted versions of channel taps and $w_k \sim \mathcal{CN}(0, \sigma^2)$.

Applying the FrDFT yields

$$r_0^{N-1} = \mathbf{F}_{N,\alpha}\, y_0^{N-1} = \mathbf{F}_{N,\alpha}\, \mathbf{H}\, \mathbf{F}_{N,\alpha}^H\, a_0^{N-1} + \mathbf{F}_{N,\alpha}\, w_0^{N-1}. \tag{7}$$

which constitutes the input to the subsequent T-Detector.

III. The Background: T-BCJR and T-Detector

In [17], the T-BCJR has been introduced as a fully trainable version of the additive SISO BCJR algorithm in which the trellis structure, the input-metric computation, and the output-LL computation are all parametrized and trainable through backpropagation of an LL-based cost function. The T-BCJR keeps the same forward–backward steps and complexity as the standard BCJR, but adds trainable ports that let gradients of cost function flow through it. This makes the whole algorithm suitable for end-to-end, iterative trainable decoding networks.

In [15], [16], we exploited the T-BCJR to build a trainable ISI detector (T-Detector) based on the channel-shortening principle [18]. The shortener-BCJR is built on the idea of having a fixed trellis structure (to maintain a reasonable complexity even if both the channel memory and the modulation cardinality increase) preceded by a shortening filter whose purpose is to transform the received signal in such a way that the reduced memory BCJR trellis detector can achieve the maximum information rate possible. The classical shortener–BCJR structure is replaced by a trainable convolutional shortener and the T-BCJR, whose branch-metric computation is parameterized by learnable matrices. All components are jointly optimized from a conditional-entropy cost function applied to the output LLs, using interspersed pilots to generate the training gradients. This allows the T-Detector to learn the optimal shortening and metric parameters without explicit CSI and to track slowly time-varying channels with performance comparable to ideal channel and modulation aware detectors.

Fig. 3 illustrates the T-Detector architecture. A trainable convolutional linear layer of length L_F first operates as a learnable channel shortener, producing the signal z. This signal is then processed by the T-BCJR module, with trellis memory L_T (lower than the channel memory), which outputs the bit (or symbol) LLs π_u^O. These LLs can be passed to a subsequent

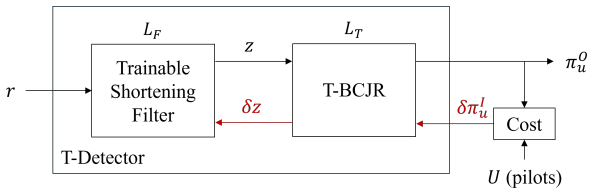

Fig. 3: The adaptive T-Detector.

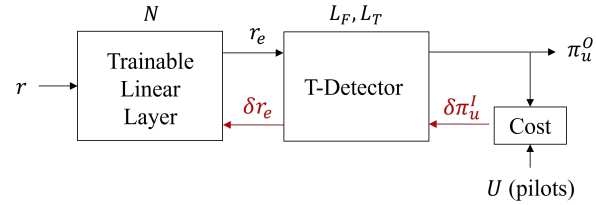

Fig. 4: T-Detector preceded by an additional trainable linear layer for channel equalization.

decoder and are also fed to the cost-function block, which generates the gradients $\delta\pi_u^I$ used to train the whole network. The trellis comprises $S = 2^{m \cdot L_T}$ states, where m denotes the modulation efficiency. Each state is connected through $E = 2^{m \cdot (L_T+1)}$ edges.

IV. The T-Detector for ICI in fading channels

The T-Detector introduced in Section III was originally designed to mitigate time-domain ISI. The same architecture, however, can be reinterpreted to handle frequency-domain ICI in SEFDM. It builds on the trellis-based approach to SEFDM detection proposed in [4]. There, the ICI structure is interpreted as a finite-state machine, and a MAP algorithm is applied to the received frequency-domain samples. As shown in Eq. 4-5 and Fig. 2, coefficients $g_{n,k}$ decay with subcarrier distance at a rate depending on α. By retaining only the K nearest neighbors, the ICI can be approximated as a finite-memory filter, enabling trellis-based sequence detection with $S = 2^{m \cdot K}$ states. While this solution achieves optimal performance, its computational complexity is prohibitively high, rendering it computationally infeasible in practice. The T-Detector adopts the same principle, but replaces the fixed matched filter with known coefficients by a trainable shortening filter of length L_F that compresses the ICI energy into a shorter window manageable by the T-BCJR with trellis memory L_T. This keeps complexity fixed at $S = 2^{m \cdot L_T}$ states, while preserving near-optimal detection and correct soft outputs for the outer decoder. The filter length L_F and trellis memory L_T are chosen based on how many adjacent subcarriers contribute significantly to the ICI, and therefore depend primarily on α.

This approach is also extended to frequency-selective channels, where the channel's frequency response varies across the bandwidth, causing each subcarrier to experience a different amplitude and phase shift. In conventional OFDM, this residual effect is handled by a one-tap frequency-domain equalizer (FDE) that compensates each subcarrier independently. In SEFDM, this impairment coexists with ICI, but the two are structurally separable: fading acts as a per-subcarrier multiplicative term, while ICI stems from the non-orthogonal subcarrier spacing and is independent of the channel realization. This separability has no counterpart in the original time-domain T-Detector. Here, it motivates the introduction of a dedicated trainable linear layer prior to the shortening filter, which applies a distinct complex gain to each subcarrier, playing the same role as a conventional one-tap FDE in OFDM. Unlike a classical equalizer, however, this layer is not derived from an explicit channel estimate: it is optimized jointly with the shortening filter and the T-BCJR through end-to-end backpropagation. Its output is then passed to the shortening filter, which continues to operate at the single-sample level to address the residual ICI. The resulting architecture is illustrated in Fig. 4.

Formally, given a received SEFDM symbol of length N, the trainable linear layer (i.e., a 1-tap equalizer) computes:

$$r_{e,0}^{N-1} = g \odot r_0^{N-1}, \tag{8}$$

where r_0^{N-1} denotes the received SEFDM symbol vector, and g is a trainable complex-valued weight vector.

A key advantage of the T-Detector architecture lies in its full trainability through backpropagation from its output LLs. Gradients from the cost function can be propagated backward through all processing stages. Specifically, the cost function output $\delta\pi_u^I$ serves as the input to the T-BCJR, whose output δz updates the shortening filter. The shortening filter, in turn, produces δr_e, which can be further backpropagated to update the coefficients of the trainable 1-tap equalizer g as follows:

$$\delta g = \delta r_{e,0}^{N-1} \odot r_0^{N-1}. \tag{9}$$

V. Considerations and limitations

The following considerations complement the architectural description in Section IV, addressing the relationship between the proposed approach and conventional equalization, the distinction between implicit and explicit channel learning, and the fundamental limits of the T-Detector in terms of compression factor and block processing.

a) Implicit channel learning vs. explicit CSI: unlike explicit-CSI schemes such as [5], [11]–[13], where pilots are used to compute a channel estimate fed into a known detection formula, the T-Detector uses pilots solely to generate gradients that update the detector (equalizer, shortening filter and T-BCJR) weights through backpropagation. The training overhead, i.e., the number of pilots required for convergence, is comparable to that of an explicit estimator; however, the implicit approach makes no parametric assumption about the channel model, making it inherently robust to model mismatch. Regarding adaptation to time-varying channels, the two approaches are analogous: an explicit estimator must refresh the channel estimate at a rate set by the coherence time, while the T-Detector requires refreshing the weights at the same rate: the difference lies in what is updated (a closed-form estimate versus a gradient step), not in how often.

b) Joint optimization of the trainable equalizer: although g shares its functional form with a conventional FDE, its joint optimization with the shortening filter and the T-BCJR means it does not converge to the isolated ZF/MMSE solution, but to whatever minimizes the overall detection cost given the subsequent stages. A direct consequence is that the converged value of g depends not only on the channel realization, but also on L_F, L_T and the modulation order m.

c) Complexity and performance limits: trellis complexity grows exponentially, so only a limited increase in memory is computationally affordable. For small α, the ICI spreads over more subcarriers and a non-negligible fraction of interference energy inevitably falls outside any practically affordable window. This effect manifests as a saturation of the achievable MI below the theoretical bound m/α.

d) Block boundary effects: a further limitation specific to the frequency-domain reinterpretation of the shortening filter concerns the boundary subcarriers of each SEFDM symbol. The ICI coefficients $g_{n,k}$ characterize interference within a single transmitted block; however, a shortening filter implemented as a sliding-window convolution across the subcarrier index k does not, by construction, respect the block boundary. Near $k = 0$ and $k = N - 1$, the filter window extends into the subcarriers of the adjacent SEFDM symbol, introducing a boundary-localized source of error that is conceptually distinct from the residual in-block ICI discussed above, and that becomes more pronounced as L_F increases. Mitigating this effect, for instance through edge-aware filtering, symbol-boundary padding, or guard subcarriers, is left as a direction for future work.

VI. Simulation Results

In this section, we assess the performance of the proposed T-Detector in SEFDM systems through a series of analyses.

We first examine the mutual information (MI) results shown in Fig. 5. The proposed T-Detector (red curves) is compared with the parallel-branch message passing algorithm (PBMPA) [13] (green curves) over an AWGN channel without CP, using $N = 64$ subcarriers, three modulations, BSPK, QPSK and 8PSK ($m = 1, 2, 3$ bits/symbol, respectively) and two compression factors, $\alpha = 0.75$ (dashed curves) and $\alpha = 0.8$ (solid curves). The T-Detector employs a shortening filter memory varying between $L_F = 4$ and $L_F = 8$ and a trellis memory $L_T = 1$. Since the channel is static, only a short initial training phase is required, with no retraining afterward. PBMPA is selected as the benchmark, as it has been shown in [13] to outperform other SEFDM-specific detectors, including the FSD method [11] and the GMP-based detector in [12]. For $\alpha = 0.8$, both detectors exhibit similar behavior, approaching the maximum achievable MI at an SNR of approximately 5dB for BPSK, 10 dB for QPSK and 20 dB for 8PSK. When the compression factor is reduced to 0.75, a similar trend is observed; however, a performance gap emerges. For QPSK, PBMPA suffers a noticeable degradation, whereas the proposed T-Detector remains robust to the increased compression, outperforming the benchmark. MI

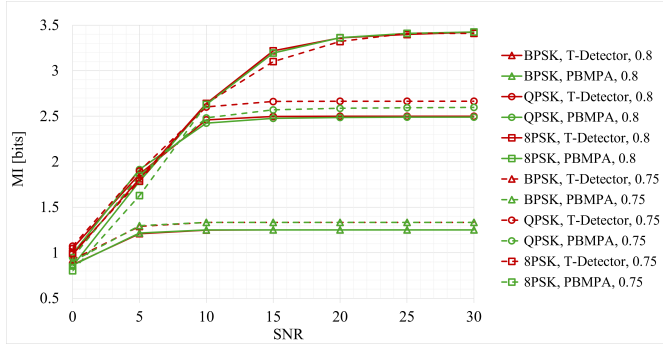

Fig. 5: MI vs SNR comparison between T-Detector and PBMPA [13] in AWGN channel for $N = 64$, BPSK (triangles), QPSK (circles) and 8PSK (squares)
and $\alpha = 0.75$ (dashed curves) and $\alpha = 0.8$ (solid lines).

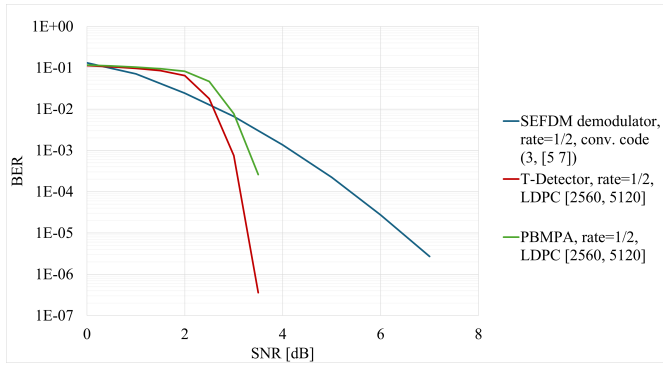

Fig. 6: BER vs SNR comparison among T-Detector, PBMPA [13] and SEFDM demodulator [4] in AWGN channel for $\alpha = 0.75$, QPSK and $N = 256$.

provides an accurate estimate of the maximum achievable outer code rate that guarantees reliable communication. For this reason, MI is adopted as the primary metric to assess detector performance.

Motivated by these results, we next present a bit-error-rate (BER) comparison in Fig. 6. The MI curves for QPSK modulation (circle markers in Fig. 5) indicate that a coding rate of $R_C = 1/2$ is well matched to both detectors and consistent with the spectral efficiency of SEFDM at $\alpha = 0.75$. Following the evaluation setup of [4], we again consider an AWGN channel without CP, $N = 256$ subcarriers, and $\alpha = 0.75$. The benchmark in [4] (blue curve) consists of an iterative SEFDM demodulator combined with convolutional coding (rate $1/2$), interleaving, and max-log-MAP decoding, using a block length of approximately 2000 bits. We compare the reference against PBMPA (green curve) and our T-Detector (red curve), both paired with an LDPC decoder of rate $R_c = 1/2$ and block length 5120. We adopt Bit-Interleaved Coded Modulation (BICM) to interface the detectors with the LDPC decoder without iterative detection. The use of Gray-labeled constellations ensures that the resulting BICM loss remains negligible. As shown in Fig. 6, both the T-Detector and PBMPA outperform the benchmark from [4]. The plot demonstrates that

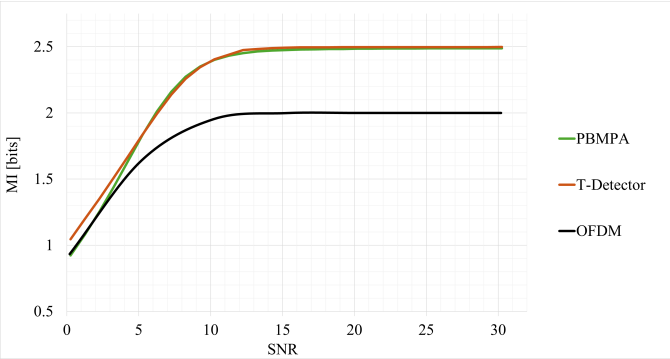

Fig. 7: MI vs SNR comparison among T-Detector, PBMPA [13] with $\alpha = 0.8$ and classic OFDM in TDL-A channel for $N = 64$ and QPSK.

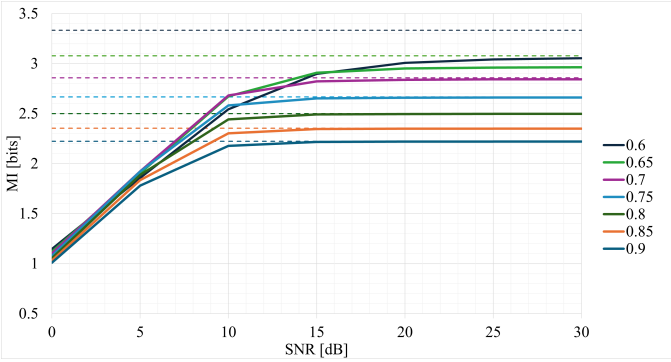

Fig. 8: MI vs SNR of the T-Detector in AWGN channel for different values of α.

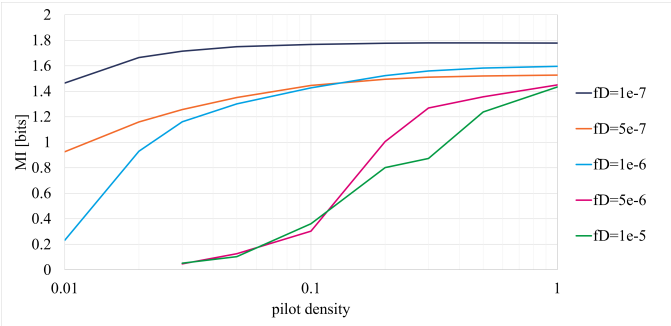

Fig. 9: MI vs pilot density of T-Detector in TDLA channel for QPSK, $\alpha = 0.8$ and different normalized Doppler frequencies f_D.

the code's performance aligns with the MI-based predictions observed in Fig. 5: when the MI reaches the transmitter SE ($\mathrm{SE_{TX}}$) of $\mathrm{SE_{TX}} = m \cdot R_C \cdot 1/\alpha = 2 \cdot 1/2 \cdot 1/0.75 = 1.33$, BER performances at the decoder output begin to drop.

The second set of results focuses on performance over a static fading channel. Fig. 7 reports the MI-versus-SNR comparison between the proposed T-Detector and PBMPA for $N = 64$ subcarriers, a CP of length $N_{\mathrm{cp}} = N/16$ and a compression factor $\alpha = 0.8$. The channel follows the TDL-A model specified in the 5G NR standard [20], with $L_C = 10$ taps. PBMPA is assumed to operate with ideal CSI, whereas the T-Detector does not rely on explicit CSI. However, since the channel is static, a sufficiently long initial training phase allows the T-Detector to learn the channel response, ensuring a fair comparison. As shown in Fig. 7, both detectors exhibit nearly identical performance across most SNR values, with the T-Detector exhibiting a slight advantage at low SNR values. For reference, the MI of a conventional OFDM system using only αN subcarriers is also shown. This comparison highlights the spectral-efficiency gains offered by SEFDM over conventional OFDM.

Next, we investigate the limits of the proposed T-Detector in terms of the maximum bandwidth compression it can accommodate while still approaching the maximum achievable MI at high SNR. Fig. 8 presents a MI-versus-SNR results in an AWGN channel with $N = 64$ subcarriers for several values of the compression factor α. For α in the range $0.75 - 0.9$, the T-Detector effectively mitigates the resulting ICI and approaches the theoretical MI limit. At $\alpha = 0.7$, performance remains strong, although a small gap emerges at high SNR between the achieved MI (solid line) and the theoretical bound m/α (dashed line). For lower compression factors, the degradation becomes more pronounced, indicating that the T-Detector can no longer fully compensate for the increased ICI. This degradation can be explained by the limitations already highlighted in Section V.

Finally, up to this point, we have considered a static scenario, where only an initial acquisition phase is required to train the T-Detector. To demonstrate that the proposed approach is not limited to static conditions, we now evaluate its ability to adapt to a slowly time-varying channel. In this setting, training proceeds continuously: an initial acquisition phase is followed by a tracking phase, during which pilot symbols are periodically interspersed with payload data. This allows the T-Detector's weights to adapt gradually to channel variations, rather than being retrained from scratch for each burst. To evaluate this scenario, the tap coefficients used for the static TDL-A channel in the previous experiment are replaced with Gaussian processes generated according to Jakes' spectrum [21], parameterized by a normalized Doppler frequency (normalized to the symbol rate). We assess the T-Detector's performance across different pilot densities and Doppler frequencies. The pilot density (overhead) is defined as the fraction of pilots relative to the total transmission, comprising both pilots and data. The pilot field length is set equal to that of a single SEFDM symbol in all simulations, in order to keep the pilot periodicity small. Each experiment simulates a time series of 10 million samples. Results are reported in Fig. 9, which shows the MI of the delivered LLs as a function of pilot density (logarithmic scale) for QPSK at $\mathrm{SNR} = 7$ dB and $L_T = 1$. Five normalized Doppler frequencies are considered, $f_D \in \{10^{-7}, 5 \times 10^{-7}, 10^{-6}, 5 \times 10^{-6}, 10^{-5}\}$. Although absolute MI values differ across realizations due to finite-length simulations, the overall trend shows that the pilot

overhead needed to approach the maximum achievable MI increases with f_D. For the slowest variation ($f_D = 10^{-7}$), the T-Detector approaches its saturation MI already at a pilot density below 0.03, whereas faster channel variations require denser pilot insertion to track the channel. This confirms the expected trade-off between tracking accuracy and pilot overhead, and demonstrates the T-Detector's ability to adapt to slowly time-varying channels. This adaptability, however, holds only up to a certain f_D: when the required overhead becomes too large, as for $f_D = 5 \times 10^{-6}$ and $f_D = 10^{-5}$, gradient-based weight updates are no longer sufficient, and alternative techniques are needed. In such cases, model-based NN architectures that jointly incorporate channel estimation into the predictive step should be considered.

VII. Conclusions

The T-Detector [15], [16] extends classical channel-shortening detectors into a fully trainable architecture, preserving flexibility while enabling an effective complexity-performance trade-off. Unlike conventional detectors, it does not require explicit channel estimation or optimal shortening coefficients, making it robust to channel mismatch and variations. In this work, we showed that the same architecture, originally developed for time-domain ISI, generalizes to frequency-domain ICI in SEFDM systems without any modification to its core detection procedure. The shortening filter operates on subcarriers rather than time samples, while an additional trainable linear layer separates the unknown per-subcarrier fading distortion from the deterministic ICI structure. The required filter length depends primarily on the compression factor α, since only the closest subcarriers contribute significantly to ICI. Results show that the proposed T-Detector matches or exceeds established SEFDM detection schemes in MI and BER, in both AWGN and fading channels. We identified the operational range of bandwidth compression for which the T-Detector effectively compensates ICI, and discussed its fundamental limits in terms of trellis complexity and block-boundary effects. Finally, we showed that the architecture adapts to slowly time-varying channels through continuous pilot-based tracking, with the pilot overhead scaling as expected with the Doppler frequency. However, this adaptability holds only up to a certain Doppler frequency, beyond which the pilot overhead becomes impractical and alternative, model-based architectures are needed. Future work will focus on mitigating these boundary effects, extending the operational range to lower compression factors, and developing model-based architectures capable of tracking faster time-varying channels.

Acknowledgement

This work was supported by the European Union - Next Generation EU under the Italian National Recovery and Resilience Plan (NRRP), Mission 4, Component 2, Investment 1.3, CUP E13C22001870001, partnership on "Telecommunications of the Future" (PE00000001 - program "RESTART").

References

[1] M. Rodrigues and I. Darwazeh, "A spectrally efficient frequency division multiplexing based communication system." International OFDM-Workshop, 2003.

[2] A. B. Kislitsyn, A. V. Rashich, and N. N. Tan, "Generation of SEFDM-signals using FFT/IFFT," in *International Conference on Next Generation Wired/Wireless Networking*. Springer, 2014, pp. 488–501.

[3] I. Darwazeh, H. Ghannam, and T. Xu, "The First 15 Years of SEFDM: A Brief Survey," in *2018 11th International Symposium on Communication Systems, Networks & Digital Signal Processing (CSNDSP)*, 2018, pp. 1–7.

[4] A. Rashich, A. Kislitsyn, D. Fadeev, and T. N. Nguyen, "FFT-based trellis receiver for SEFDM signals," in *2016 IEEE Global Communications Conference (GLOBECOM)*. IEEE, 2016, pp. 1–6.

[5] A. Rashich and S. Gorbunov, "ZF equalizer and trellis demodulator receiver for SEFDM in fading channels," in *2019 26th international conference on telecommunications (ICT)*. IEEE, 2019, pp. 300–303.

[6] V. T. Nguyen, A. Rashich, and C. M. Nguyen, "Pulse-Shaped SEFDM Signals in Frequency-Selective Fading Channels," in *2023 International Conference on Electrical Engineering and Photonics (EExPolytech)*. IEEE, 2023, pp. 238–241.

[7] B. Yu, H. Zhang, X. Hong, C. Guo, A. P. T. Lau, C. Lu, and X. Dai, "Channel equalisation and data detection for SEFDM over frequency selective fading channels," *IET Communications*, vol. 12, no. 18, pp. 2315–2323, 2018.

[8] S. V. Zavjalov, S. B. Makarov, S. V. Volvenko, and A. A. Balashova, "Efficiency of coherent detection algorithms nonorthogonal multifrequency signals based on modified decision diagram," in *Conference on Internet of Things and Smart Spaces*. Springer, 2015, pp. 599–604.

[9] D. Dasalukunte, F. Rusek, and V. Öwall, "An iterative decoder for multicarrier faster-than-Nyquist signaling systems," in *2010 IEEE International Conference on Communications*. IEEE, 2010, pp. 1–5.

[10] I. Kanaras, A. Chorti, M. Rodrigues, and I. Darwazeh, "Analysis of Sub-optimum detection techniques for a bandwidth efficient multi-carrier communication system," in *Cranfield Multi-Strand Conference: Creating Wealth Through Research and Innovation*, vol. 6, 2008, p. 505.

[11] S. Isam and I. Darwazeh, "Design and performance assessment of fixed complexity spectrally efficient FDM receivers," in *2011 IEEE 73rd Vehicular Technology Conference (VTC Spring)*. IEEE, 2011, pp. 1–5.

[12] Y. Ma, F. Tian, N. Wu, B. Li, and X. Ma, "A low-complexity receiver for multicarrier faster-than-Nyquist signaling over frequency selective channels," *IEEE Communications Letters*, vol. 24, no. 1, pp. 81–85, 2019.

[13] M. Mirabella, P. Di Viesti, and G. M. Vitetta, "A Novel Message Passing Algorithm for Soft-Output Detection in Faster-than-Nyquist Multicarrier Systems," in *2025 IEEE 26th International Workshop on Signal Processing and Artificial Intelligence for Wireless Communications (SPAWC)*, 2025, pp. 1–5.

[14] M. Magnaldi and G. Montorsi, "Adaptive T-Detector exploiting Outer SISO Decoder in Time-Selective Channels," in *2025 13th International Symposium on Topics in Coding (ISTC)*. IEEE, 2025, pp. 1–5.

[15] M. Magnaldi and G. Montorsi, "The RNN BCJR Detector in Time-Varying Channels," in *IEEE Wireless Communications and Networking Conference*. IEEE, Mar. 2025.

[16] M. Magnaldi and G. Montorsi, "The Trainable BCJR and Its Applications," *IEEE Transactions on Communications*, vol. 74, pp. 9561–9574, 2026.

[17] G. Montorsi and B. Ripani, "RNN BCJR: a fully trainable version of the additive BCJR algorithm," in *ICC 2023-IEEE International Conference on Communications*. IEEE, 2023, pp. 3696–3701.

[18] F. Rusek and A. Prlja, "Optimal channel shortening for MIMO and ISI channels," *IEEE transactions on wireless communications*, vol. 11, no. 2, pp. 810–818, 2011.

[19] D. D. Falconer and F. Magee Jr, "Adaptive channel memory truncation for maximum likelihood sequence estimation," *Bell System Technical Journal*, vol. 52, no. 9, pp. 1541–1562, 1973.

[20] 3GPP, "Study on channel model for frequencies from 0.5 to 100 ghz," 2018.

[21] M. J. Gans, "A power-spectral theory of propagation in the mobile-radio environment," *IEEE Transactions on Vehicular Technology*, vol. 21, no. 1, pp. 27–38, 1972.